2 Sismantilles I experiment and a-priori location

2.1 Network Layout and quality of earthquake data

In well instrumented subduction zones like the Japan arc, locations of earthquakes under the offshore forearc and the interplate megathrust seismogenic zone have been demonstrated to be grossly in error, once they obtained records of Ocean Bottom Seismometers (hereafter OBS) deployed far offshore (Hasegawa et al., 1991). Offshore Tohoku, the first OBS deployment for long-term earthquake observation had started in 1987 and continued to present with 3 permanent sensor sites cabled to the coast.

In the Lesser Antilles, between November 1999 and January 2002, a temporary field experiment, conducted by « Laboratoire de sismologie expérimentale » of the « Institut de Physique du Globe de Paris » (hereafter IPGP), has been carried out over a large region along the arc between the Martinique and Antigua islands (figure 2.1). This experiment, named SISMANTILLES I, represents the first successful attempt of a combined on-offshore seismological network in this area and was aimed to record local earthquake activity and to provide a data-set which would allow high precision earthquake location and permit the inversion for one- and three-dimensional crustal velocity structure. Several authors (see paragraph 1.3) provide information about the distribution of the seismicity in the region, these information were used to plan a temporary seismic network that complemented a local seismic network from the « Observatoire Volcanologique et Sismologique de Guadeloupe» (hereafter OVSG). 39 one-component stations equipped primarily with short period seismometers having a natural frequency of 1 Hz composed this seismic array. The seismic network of the SISMANTILLES I experiment, that covered an area of about 150 km in NEE-SWW direction and of about 300 km in NNW-SSE direction, it was composed of two parts: a landward and a seaward network, which will be described separately in the following.

The landward network was formed by 43 three components seismic stations from IPGP that operated from November 1999 to August 2000 and for a second period from November 2001 to January 2002. The deployment of IPGP seismic stations (red triangles in figure 2.1) led to an homogeneous distribution of network components, avoiding a concentration on the flanks of "La Soufrière" and "Montagne Pelée" volcanoes. With this addition, the seismic network was optimized in order to locate regional seismic events.

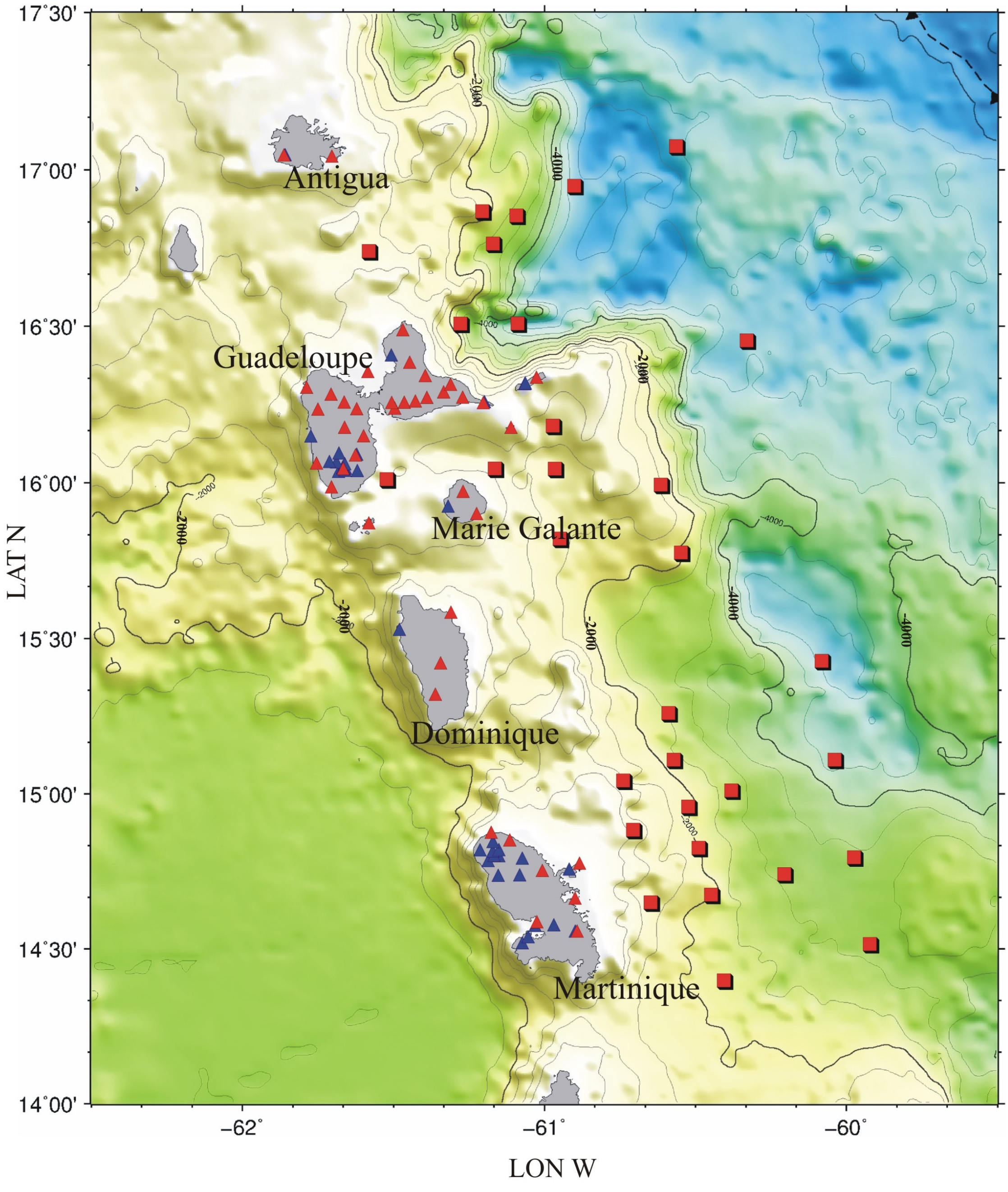

Figure 2.1: Map showing OBS and land stations used in SISMANTILLES I experiment. Blue triangles: seismic stations of OVSG. Red triangles: temporary seismic stations. Red squares: off-shore network. Bathymetry is from Smith and Sandwell (1997). The deformation front, related to the subduction of the Atlantic Ocean lithosphere beneath the Caribbean Plate, is represented by dashed line with triangles.

These temporary seismic stations were equipped with three types of recording instruments: Mini Titan HI7190, Reftek model 130-02, and Hathor3. All instruments, recording on a continuously mode with a sampling rate of 100 Hz, were equipped with a 5s (Titan and Rftek) or a 2 Hz three-component seismometer.

During the fieldwork station coordinates were taken with the GPS instruments with errors in latitude and longitude inferior to ± 10 m. Analysis of earthquake data also requires that the correct time for each data point on a seismic trace (sample) is known with certain accuracy. Indeed the kind of analysis, which can be successfully undertaken, and its quality are strongly coupled with this accuracy. In the Titan and Reftek stations the true time derive directly from GPS satellite, the seimic signal is either saved on the data records directly or used to control and update an internal clock in the recording unit which is then used to set the time on the data.On the contrary, in the Hathor stations the internal clock is not corrected with the external pulse; only the difference between internal and external time (lag) is recorded together with the internal time. The lag (figure 2.2) is then applied to correct the internal time when processing data.

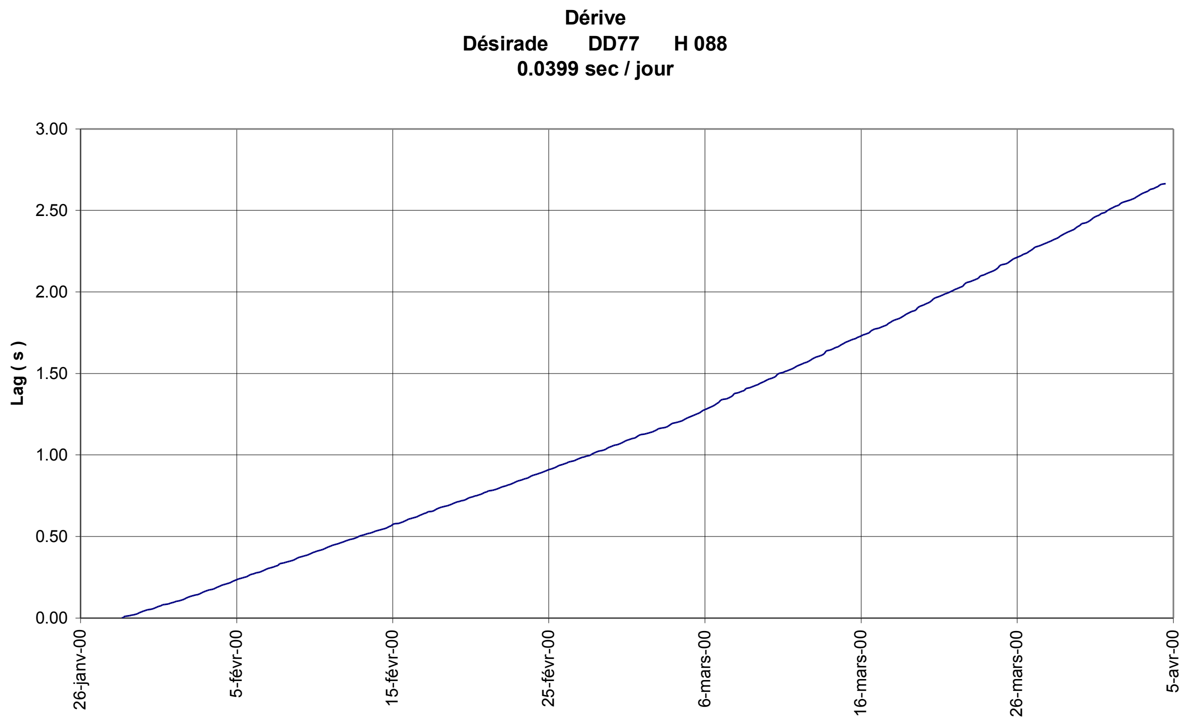

Figure 2.2: Lag value for the Desirade station in the period 26-01-2000/05-04-2000.

After a failed attempt due to ship breakdown, the landward network has been complemented by 31 OBS. These instruments were left on the seafloor for 69 days starting November 24th, 2001 to record simultaneously natural seismicity and the MCS shots from the french N/O Nadir vessel (Laigle et al., 2005).

To better locate the interplate seismicity, it was particularly important to have records of OBS located directly above the hypocentres. Indeed land stations were too far from the sources and do not allow to obtain earthquake locations with good azimuthal coverage. As observed on most of the ocean-floor observatories, the noise level at the OBS site is quite large on all components (Dahm et al., 2006). However, although a higher noise level yield gives a lower sensitivity for OBS's, one or more observations improve the azimuthal coverage and constrain a better hypocenter location. The OBS use, as in this case, is limited by their low battery life (approximately 8 weeks for continuous recording).

All OBS (figure 2.3) stations were equipped with a three-component seismometer, 9 of them (from the Institut de recherche pour le développement of Villefranche-sur-Mer - France) are characterized by short period 4.5 Hz seismometers and 22 (from the Institute of Seismology and Volcanology of Okkaido - Japan) by broadband seismometers (60s). They recorded on a continuous mode at sampling rate of 100 Hz. A linear time drift correction was applied to the data taking into account time synchronized with GPS clock just before the deployment and just after recovery of the OBS. In total 140 instruments, all running in continuous mode, were in use. All station positions used in the SISMANTILLES I experiment are shown in figure 2.1.

2.2 Determination of first arrival times

Identifying first arrival times of P- and S- waves on waveforms was done with Pickev software for Reftek and Hathor data (Fréchet et Thouvenot, 2000), with Rtoo software (elaborated by A. Nercessian of IPGP) for Titan and OBS data. To the arrival time readings of the IPGP temporary seismometers, the readings of the permanent array primarily composed of vertical component seismometer could be added by courtesy of OVSG.

Observation weights are assigned according to the Table 2.1, for the temporary network S-wave arrivals are only picked on the horizontal components because all stations are three components.

Table 2.1 : Observation weights for P- and S-waves assigned to the uncertainties of first arrival onset.

Weight	0	1	2	3
P-wave	<0.05	0.05 – 0.1	0.1 – 0.15	0.15 – 0.2
S-wave	<0.1	0.1 – 0.175	0.175 – 0.25	0.25 – 0.3

Most of the P wave arrivals were assigned a weight of 0 as they could be read with a picking accuracy lesser than 0.05 s.

Figure 2.3: OBS are autonomous instruments that sit seafloor and record waves. Floats made from glass balls and syntactic foam make each OBS buoyant, but an anchor holds it on the seafloor during the survey. Photo shows an OBS deployment.

The following table gives the list of stations and the number of times they are found into the original phases file:

NAME	Number of components - Network	Latitude	Longitude	Altitude	Total number arrivals	Number S-arrivals
MV3	3C-Temporary	14.5547N	60.8892W	355	79	38
ZA3	3C-Temporary	14.5845N	61.0227W	17	67	33
ROS	3C-Temporary	14.6600N	60.8963W	28	88	44
PROS	3C-Temporary	14.6600N	60.8963W	28	23	11

BONA	3C-Temporary	14.7493N	61.0043W	197	26	13
AIR	3C-Temporary	14.7493N	61.0043W	197	59	29
CAR	3C-Temporary	14.7723N	60.8817W	124	24	12
LEY	3C-Temporary	14.8468N	61.1123W	136	33	16
BSJ	3C-Temporary	14.8718N	61.1737W	135	29	14
OPH	3C-Temporary	15.3148N	61.3590W	107	62	28
PEN	3C-Temporary	15.4148N	61.3417W	304	176	81
WES	3C-Temporary	15.5775N	61.3077W	40	193	88
SAIN	3C-Temporary	15.8647N	61.5795W	0	118	59
PERE	3C-Temporary	15.8938N	61.2227W	24	185	89
GRE	3C-Temporary	15.9655N	61.2678W	70	173	84
OBS	3C-Temporary	15.9798N	61.7032W	408	125	56
GALI	3C-Temporary	16.0387N	61.6645W	1140	25	10
GDE	3C-Temporary	16.0565N	61.7528W	55	30	15
BRI	3C-Temporary	16.0823N	61.6237W	432	205	102
DOUV	3C-Temporary	16.1438N	61.5967W	100	151	74
PTT	3C-Temporary	16.1707N	61.1093W	8	43	21
VERN	3C-Temporary	16.1713N	61.6602W	221	117	55
ESPE	3C-Temporary	16.2295N	61.7480W	148	316	157
RETR	3C-Temporary	16.2307N	61.6197W	44	142	70
BARB	3C-Temporary	16.2323N	61.4942W	70	411	196
CHA	3C-Temporary	16.2503N	61.2007W	9	63	25
TER	3C-Temporary	16.2505N	61.5037W	43	34	17
TASS	3C-Temporary	16.2512N	61.4622W	63	296	142
DONO	3C-Temporary	16.2518N	61.6615W	55	6	3
ZABR	3C-Temporary	16.2550N	61.4257W	109	158	78
LOU	3C-Temporary	16.2667N	61.3878W	36	147	69
AERO	3C-Temporary	16.2673N	61.2688W	31	45	21
BIS	3C-Temporary	16.2772N	61.7047W	130	209	95
CELC	3C-Temporary	16.2847N	61.3318W	34	287	130
NTRD	3C-Temporary	16.2993N	61.7857W	148	201	98
BLMA	3C-Temporary	16.3092N	61.3093W	31	204	92
DESI	3C-Temporary	16.3317N	61.0250W	177	262	127
NERO	3C-Temporary	16.3367N	61.3932W	48	180	85
FAJ	3C-Temporary	16.3500N	61.5833W	0	152	75
DANJ	3C-Temporary	16.3798N	61.4442W	4	268	128
HYP	3C-Temporary	16.4840N	61.4672W	33	227	98
FRE	3C-Temporary	17.0412N	61.7023W	82	319	158
BOG	3C-Temporary	17.0450N	61.8613W	367	335	155
BIMZ	1C-Permanent	14.5170N	61.0708W	425	356	126
MBIG	1C-Permanent	14.5170N	61.0708W	425	24	12
TRMZ	1C-Permanent	14.5363N	61.0512W	78	249	58
MVMZ	1C-Permanent	14.5545N	60.8955W	361	316	92
ZAMZ	1C-Permanent	14.5727N	61.0287W	25	360	111
LPMZ	1C-Permanent	14.5745N	60.9663W	130	325	83
FDFZ	3C-Permanent	14.7333N	61.1503W	510	472	213
BVMZ	1C-Permanent	14.7350N	61.0797W	694	291	75
CRMZ	1C-Permanent	14.7537N	60.9155W	180	307	94

MLMZ	1C-Permanent	14.7810N	61.1838W	370	251	45
MJMZ	1C-Permanent	14.7887N	61.0708W	400	52	18
PCMZ	1C-Permanent	14.7968N	61.1487W	730	211	47
GBMZ	1C-Permanent	14.7973N	61.1648W	800	357	107
LAMZ	3C-Permanent	14.8113N	61.1685W	1240	303	107
CPMZ	1C-Permanent	14.8155N	61.2105W	335	341	90
BAMZ	1C-Permanent	14.8157N	61.1483W	670	391	125
SAMZ	1C-Permanent	14.8417N	61.1678W	510	122	22
BBLZ	1C-Permanent	15.5230N	61.4780W	365	91	5
MGGZ	1C-Permanent	15.9180N	61.3168W	51	135	1
PAGZ	1C-Permanent	16.0297N	61.6800W	670	173	37
DOGZ	1C-Permanent	16.0320N	61.6178W	460	193	1
LKGZ	1C-Permanent	16.0328N	61.6583W	1380	69	7
ECGZ	1C-Permanent	16.0400N	61.6572W	1406	42	0
TAGZ	1C-Permanent	16.0420N	61.6642W	1182	316	113
RMGZ	1C-Permanent	16.0443N	61.6657W	1150	70	0
CAGZ	1C-Permanent	16.0542N	61.6592W	1370	139	3
FNGZ	1C-Permanent	16.0603N	61.6867W	825	199	1
MOGZ	1C-Permanent	16.0613N	61.7103W	640	147	4
BRGZ	1C-Permanent	16.0850N	61.6197W	442	140	2
STGZ	1C-Permanent	16.0887N	61.6788W	1210	6	1
LZGZ	1C-Permanent	16.1430N	61.7720W	97	156	3
SFGZ	1C-Permanent	16.2533N	61.1965W	10	35	0
MONT	1C-Permanent	16.3112N	61.0638W	303	53	26
DEGZ	1C-Permanent	16.3132N	61.0618W	275	520	218
SEGZ	1C-Permanent	16.4028N	61.5052W	60	147	2
BPAZ	1C-Permanent	17.0460N	61.8570W	396	15	1
SLBZ	1C-Permanent	13.8258N	61.0408W	600	0	0
OBSZ	1C-Permanent	14.7333N	61.1503W	510	0	0
PAMZ	1C-Permanent	14.6138N	61.0363W	120	0	0
ABGZ	1C-Permanent	16.0323N	61.6603W	1150	0	0
EGCZ	1C-Permanent	16.0302N	61.6538W	1395	0	0
FBGZ	1C-Permanent	15.9678N	61.6487W	185	0	0
HMGZ	1C-Permanent	15.9707N	61.7000W	420	2	1
MLGT	1C-Permanent	16.7250N	62.1623W	287	0	0
MLGZ	1C-Permanent	16.7250N	62.1623W	287	83	5
MSGZ	1C-Permanent	16.0987N	61.7220W	851	0	0
PRGZ	1C-Permanent	16.0362N	61.6622W	1070	0	0
MDNZ	1C-Permanent	15.3160N	61.4000W	99	0	0
NEVZ	1C-Permanent	17.1360N	62.5710W	244	0	0
SLWZ	1C-Permanent	14.0200N	60.9360W	366	29	8
CHAZ	1C-Permanent	13.8583N	61.0643W	242	0	0
MCAZ	1C-Permanent	13.8503N	61.0190W	615	0	0
MSPT	1C-Permanent	16.6910N	62.2000W	106	0	0
H5BZ	1C-Permanent	14.4250N	60.8367W	10	20	8
H5AZ	1C-Permanent	16.3133N	61.0605W	255	1	0
CPB	1C-Permanent	17.6400N	61.8260W	5	0	0
MJHT	1C-Permanent	16.7672N	62.1697W	1870	0	0

MRYT	1C-Permanent	16.7038N	62.1532W	355	0	0
MGHZ	1C-Permanent	16.7200N	62.2158W	351	0	0
MDN	1C-Permanent	15.3185N	61.3923W	99	0	0
DBCT	1C-Permanent	15.2708N	61.3455W	527	0	0
DPMT	1C-Permanent	15.2608N	61.3770W	50	0	0
BEAU	1C-Permanent	14.8718N	61.1737W	0	0	0
LPLZ	1C-Permanent	14.5745N	60.9663W	130	4	0
TRLZ	1C-Permanent	14.5363N	61.0512W	78	3	0
LALZ	3C-Permanent	14.8113N	61.1685W	1240	4	1
ob03	3C- OBS	16.9410N	60.8960W	-982	26	10
ob05	3C- OBS	16.7560N	61.1648W	-1900	41	17
ob06	3C- OBS	16.8460N	61.0875W	-1588	39	17
ob08	3C- OBS	16.4990N	61.2725W	-1606	51	23
ob16	3C- OBS	15.9998N	61.5167W	-4072	55	22
ob19	3C- OBS	16.0332N	60.9598W	-3253	29	8
ob21	3C- OBS	15.9820N	60.6090W	-2845	29	13
ob25	3C- OBS	15.7640N	60.5420W	-2398	38	19
obs26	3C- OBS	15.2493N	60.5833W	-1700	149	67
obs29	3C- OBS	15.0328N	60.7328W	-3730	44	27
obs30	3C- OBS	15.0998N	60.5658W	-2097	52	27
obs32	3C- OBS	14.9493N	60.5172W	-2535	99	44
obs33	3C- OBS	15.0010N	60.3748W	-1590	51	26
j01	3C- OBS	16.7318N	61.5757W	-3624	94	36
j02	3C- OBS	16.8593N	61.2005W	-2424	98	40
j04	3C- OBS	17.0682N	60.5587W	-709	42	5
j09	3C- OBS	16.4995N	61.0828W	-301	85	36
j13	3C- OBS	16.1713N	60.9665W	-3482	23	11
j15	3C- OBS	16.4448N	60.3248W	-696	81	23
j18	3C- OBS	16.0342N	61.1588W	-3316	129	63
j20	3C- OBS	15.8093N	60.9438W	-2948	178	81
j27	3C- OBS	15.4167N	60.0757W	-708	43	21
j31	3C- OBS	14.8745N	60.6998W	-3680	114	52
j35	3C- OBS	15.0997N	60.0332W	-196	27	15
j36	3C- OBS	14.8172N	60.4835W	-2483	0	0
j37	3C- OBS	14.6423N	60.6418W	-3348	47	27
j38	3C- OBS	14.6667N	60.4413W	-2048	0	0
j39	3C- OBS	14.7328N	60.1997W	-1182	40	23
j40	3C- OBS	14.7862N	59.9682W	-954	37	22
j41	3C- OBS	14.3917N	60.3995W	-2130	39	21
j42	3C- OBS	14.5083N	59.9163W	-1303	28	18
j22	3C- OBS	16.0314N	60.2164W	-4100	28	10

Table 2.2: List of stations with the number of observed arrival times.

Our data base comprises about 15,500 arrival readings. The S-wave readings, read primarily on horizontal components, are about 5,700.

2.3 The a-priori velocity models

A major feature of the Lesser Antilles region is the high-gradient crustal thinning from the Caribbean island arc (~30 km) to the North American Plate (~15 km) (Roux, 2007). For this reason, we consider two 1-D a priori models derived from the studies of Dorel et al. (1974) and from seismic refraction profiles of the Ladle Study Group (1983):

Model 1 (Dorel, 1981) : 3.5 km/s (depth -3.0 3.0 km), 6.0 km/s (depth 3.0 15.0 km), 7.0 km/s (depth 15.0 30.0 km), 8.0 (depth >27.0 km)

Model 2 (Ladle Study Group, 1983): 3.5 km/s (depth -3.0 3.0 km), 6.0 km/s (depth 3.0 15.0 km), 8.0 (depth >15.0 km).

In the model 1, with regard to the Moho depth, we consider the results obtained by Kopp et al. 2011. The Vp/Vs value is very important for the hypocenter determination. An example is provided by two earthquakes with many observations occurred to the east of Dominique Island. If Vp/Vs value changes from 1.85 to 1.75 we note differences in the source depth in the order 10-20 kms for the deeper events (figure 2.5). Evidently we have a minor influence of the different Vp/Vs ratios for the determination of focal depth for the shallower events. On the basis of a recent analysis of OSVG data-base (Clément, 2001), the value of 1.76, determined via Wadati diagrams, have been chosen as initial Vp/Vs ratio.

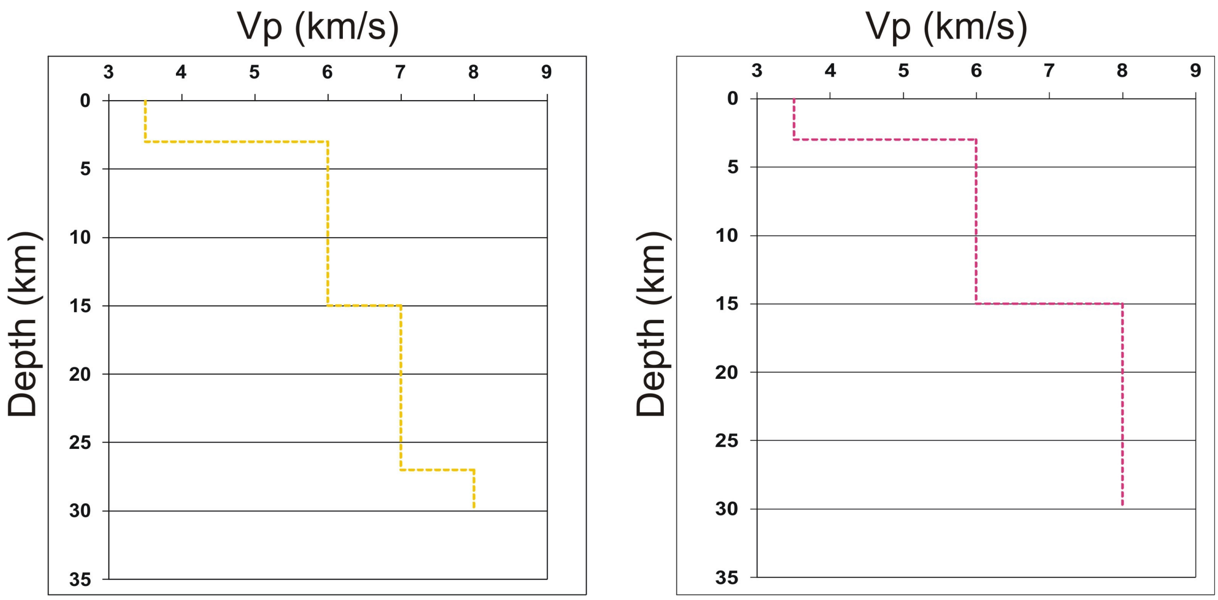

Figure 2.4: The two a-priori 1-D velocity models used in this study. On the left Model 1 of Dorel et al. (1974). On the right the Model 2 (Ladle Study Group, 1983).

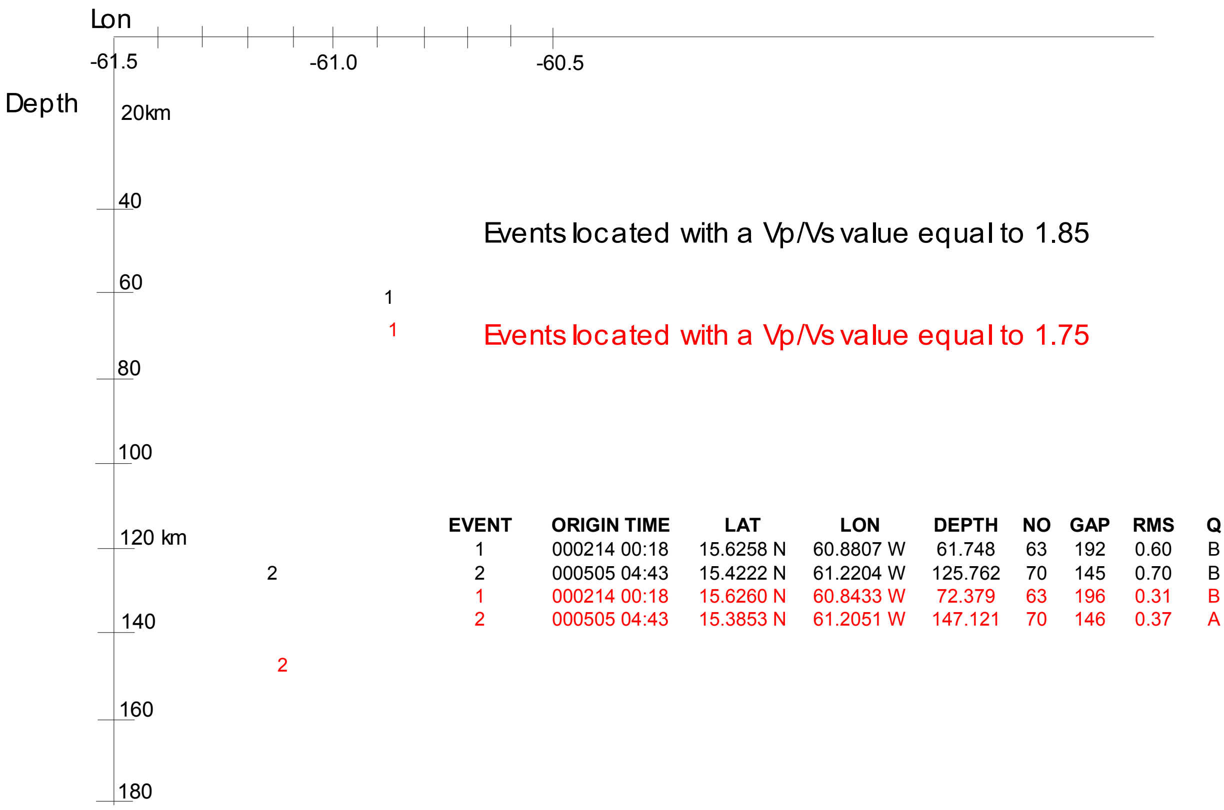

EVENT	ORIGIN TIME	LAT	LON	DEPTH	NO	GAP	RMS	Q
1	000214 00:18	15.6258 N	60.8807 W	61.748	63	192	0.60	B
2	000505 04:43	15.4222 N	61.2204 W	125.762	70	145	0.70	B
1	000214 00:18	15.6260 N	60.8433 W	72.379	63	196	0.31	B
2	000505 04:43	15.3853 N	61.2051 W	147.121	70	146	0.37	A

Figure 2.5: E-W cross section of hypocenters computed by using the programme VELEST and the 1-D velocity model proposed by Dorel et *al.* (1974). These events are located with Vp/Vs value equal to 1.85 (black) and to 1.76 (red).

2.4 The use of S- wave readings in hypocenter locations

In this section we emphasize as the use of S-wave readings is very important to obtain good hypocentre locations. As figure 2.6 shows, the S-wave readings are often not possible if we dispose of only one-component seismic stations, like in the case of the OVSG permanent network.

Since the sensors of seismic arrays are currently placed at or near the topographical surface, if the horizontal aperture of the array is chosen, its vertical extension is restrained. From simple geometrical considerations, the array resolution power for source location is better for the horizontal coordinates and that on the vertical one decreases with increasing depth. However if two waves emitted simultaneously from the source propagate with different velocities, each sensor resolves the range and hypocentral depth receives an additional constraint (Hirn et *al.*, 1991).

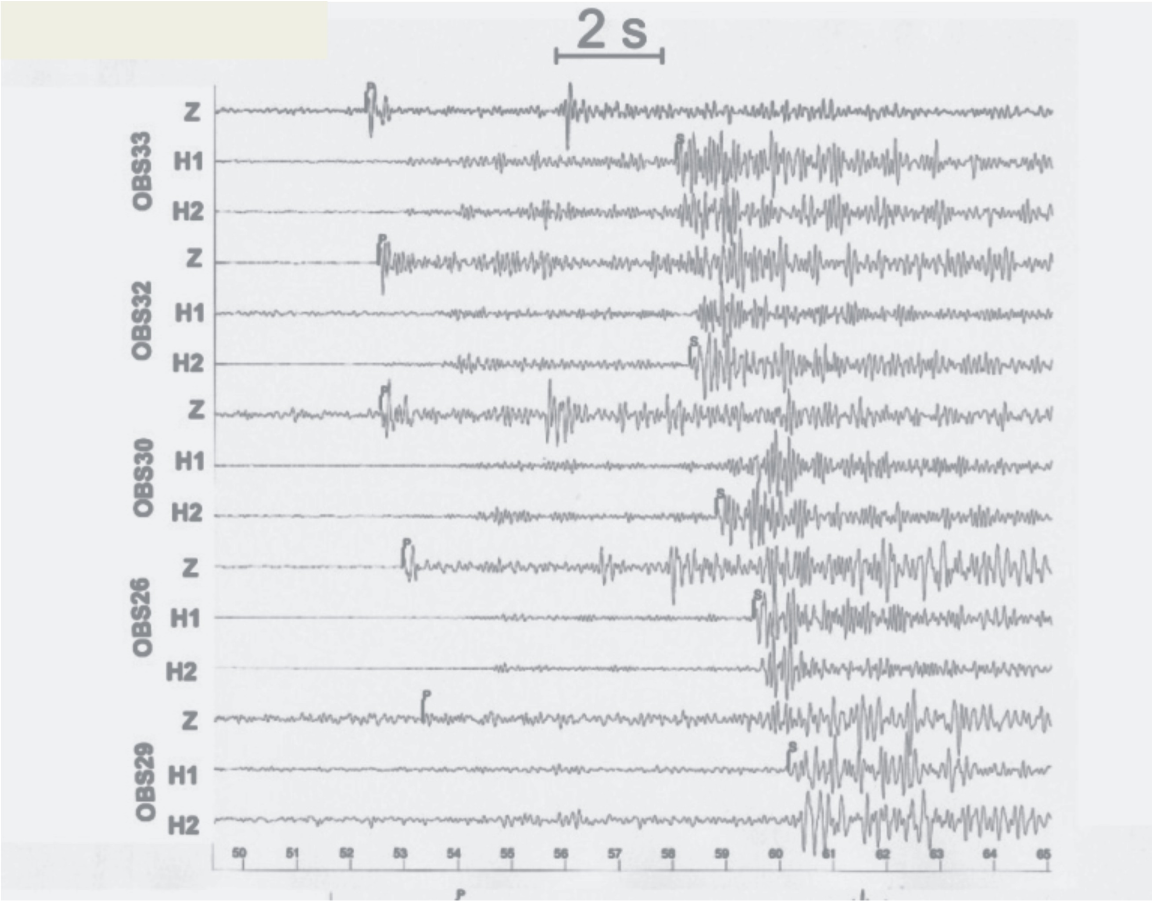

Figure 2.6: Typical records of an event obtained by five OBS. High quality of S-waves readings obtained thanks to the horizontal components of OBS. These events have been located at more than 40 km depth. In the absence of the horizontal components, the S waves would have been picked on the vertical sensor with an error of about 2 seconds due to the strong P to S converted waves.

An example is provided by the two earthquakes of figure 2.5 occurred to the east of Dominique Island. If only P arrivals are used we note very little differences in horizontal location but a big shift, from 10 to 35 km, of the hypocenter depth (figure 2.7). That these hypocenters are incorrect are not evident from formal errors of the VELEST output file on the hypocenter locations (Kissling, 1995), rms values in fact increase from less than 0.3 s to 0.6-0.7 s by the addition of S-wave observations. Another example is provided by a multiplet of seven events occurred between Guadeloupe and Antigua Island. A multiplet is a group of seismic events with very similar waveforms, despite different origin times (figure 2.8). Many studies assert that waves generated by similar sources, propagating along similar paths, will generate similar waveforms and likely a multiplet is the expression of stress release on the same structure (Fremont et Malone, 1987).

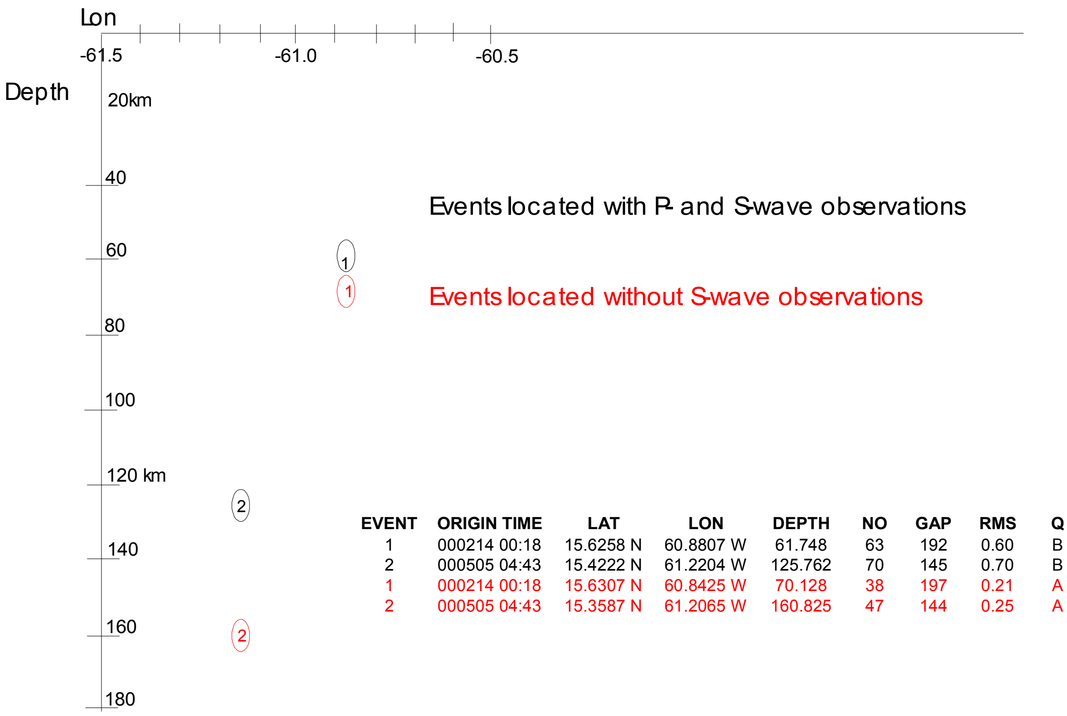

EVENT	ORIGIN TIME	LAT	LON	DEPTH	NO	GAP	RMS	Q
1	000214 00:18	15.6258 N	60.8807 W	61.748	63	192	0.60	B
2	000505 04:43	15.4222 N	61.2204 W	125.762	70	145	0.70	B
1	000214 00:18	15.6307 N	60.8425 W	70.128	38	197	0.21	A
2	000505 04:43	15.3587 N	61.2065 W	160.825	47	144	0.25	A

Figure 2.7: E-W cross section of two hypocenters computed with P- and S-wave observations (black) and with only first arrivals (red). These events are located by using the programme VELEST and the 1-D velocity model proposed by Dorel et *al.* (1974).

In figure 2.8 we can note a constant interval between P and S arrivals and also similar wave shapes which constrain the sources to be at a same depth and very tightly clustered. If only P arrivals are used, the events spread over a volume that is elongated by more than 10 km in depth (figure 2.9).

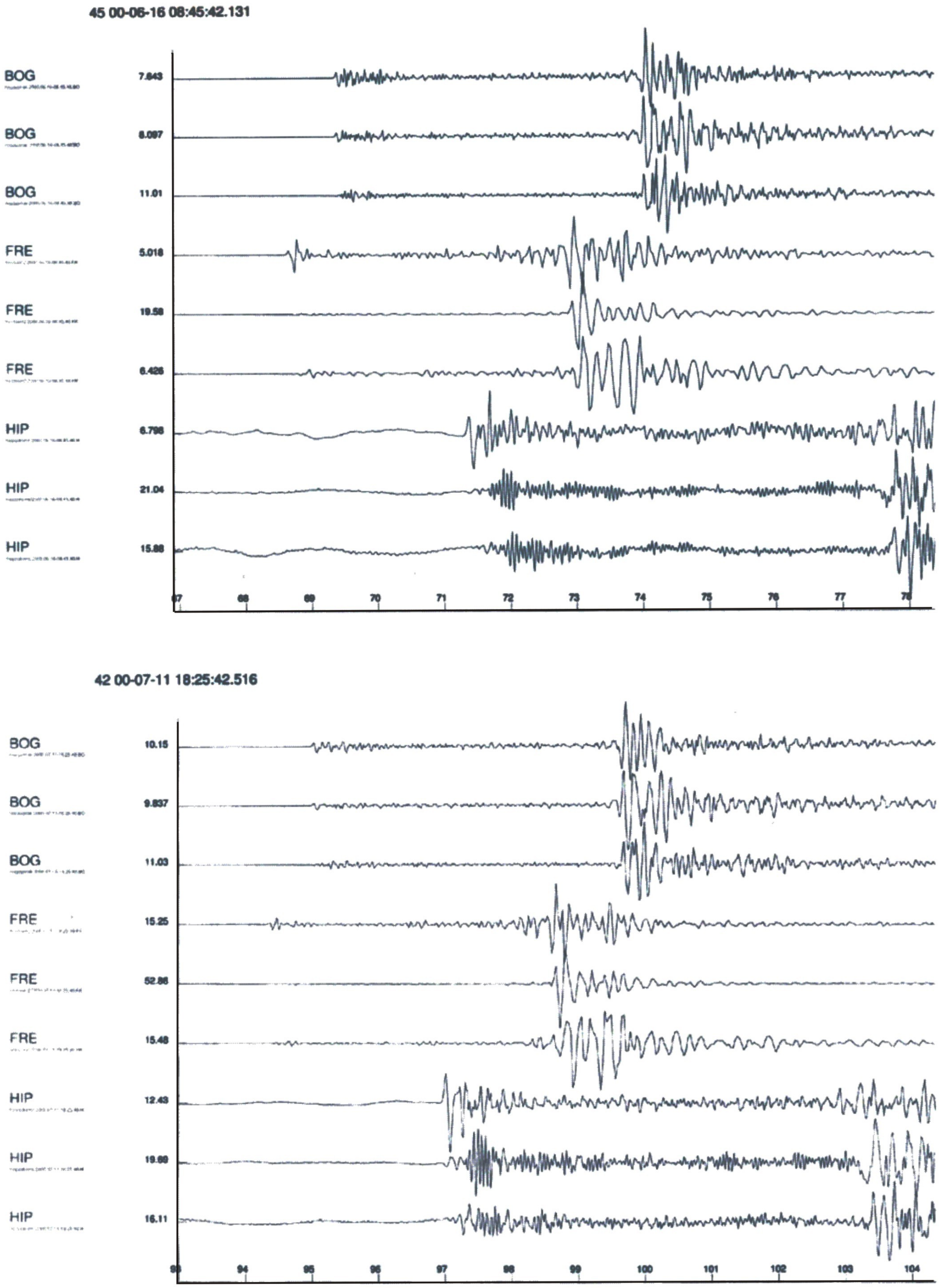

Figure 2.8: Two seismograms from the multiplet of seven events occurred on July 2000 between Antigua and Guadeloupe Island. Note constant interval between P and S arrivals and also similar wave shapes.

Also in this example, that the hypocenters located without –S readings are incorrect are not evident from formal errors of the output file on the hypocenter locations, rms values in fact increase from less 0.3 s to 0.3-0.6 s by the addition of S-wave observations. Therefore we may have a more precise location only by adding good S readings.

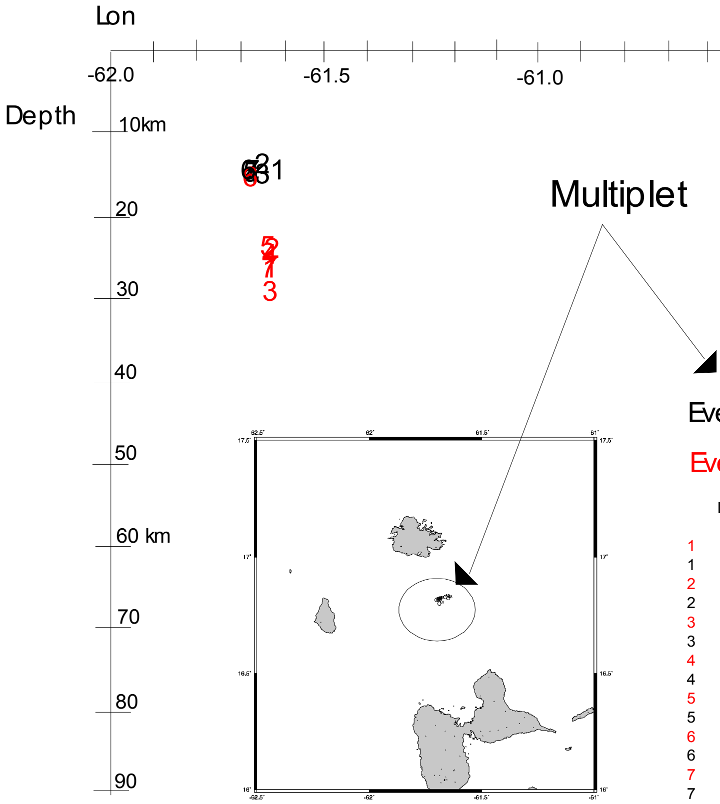

Events located with P- and S-wave observations

Events located without S-wave observations

	DATE	ORIGIN	LAT	LON	DEPTH	NO	GAP	RMS	Q
1	000305	08:00	16.8493 N	61.6576 W	26.821	19	142	0.24	A
1	000305	08:00	16.8238 N	61.6492 W	15.861	28	142	0.61	C
2	000306	21:47	16.8456 N	61.6691 W	25.005	13	141	0.08	A
2	000306	21:47	16.8202 N	61.6909 W	15.050	18	131	0.35	B
3	000317	05:44	16.8332 N	61.6503 W	30.017	7	145	0.10	A
3	000317	05:44	16.8006 N	61.6878 W	15.929	14	140	0.27	B
4	000404	11:39	16.8482 N	61.6742 W	25.801	18	174	0.15	B
4	000404	11:39	16.8161 N	61.6931 W	15.095	29	164	0.41	C
5	000616	08:46	16.8384 N	61.6817 W	24.138	17	154	0.19	A
5	000616	08:46	16.8162 N	61.7010 W	14.863	29	145	0.41	B
6	000711	18:26	16.8297 N	61.6534 W	15.085	20	141	0.33	B
6	000711	18:26	16.8286 N	61.6601 W	14.880	32	138	0.42	B
7	000726	23:29	16.8475 N	61.6656 W	26.489	18	139	0.19	A
7	000726	23:29	16.8201 N	61.6847 W	15.158	31	135	0.44	B

Figure 2.9: Map location and E-W cross section of a multiplet computed with P- and S-wave observations (black) and with only first arrivals (red). These events are located by using the programme VELEST and the 1-D velocity model proposed by Dorel et *al.* (1974).

2.5 The earthquake selection for the 1-D inversion

Our SISMANTILLES I data base comprises almost 1,000 earthquakes with an average number of observations for event equal to 15.7. In this step, we obtain the a-priori location by using VELEST (Kissling, 1995) in single-event mode. Successively, in the second step of LET, we read, by using the same software but in simultaneous mode, the input files with the selected best events. In this step of inversion process, to assess the unknown parameters, the norm of the misfit function is minimized in a least squares sense. This means that, although this method is robust, large residuals are overweighs and are likely to bias the process. This norm insures robustness but, in exchange, it overweighs large residuals that will bias the final results.

For our purpose, we selected only well located events matching minimum requests with respect to location quality:

◊ the events located with less than 14 observations, of which at least 2 S-wave readings, are discarded;

◊ the maximum *rms* for an event is 0.5 s, if the number of observations is inferior to 40, and 1.0, if the observations are superior to 40;

◊ the maximum GAP, the largest angular distance between two neighboring stations as seen from the epicenter, is 220° if the number of observations is superior to 30 and with at least 6 S-wave readings; 180° if the number of observations is inferior to 30;

◊ if two or more events are located in the same area, we select the earthquakes with a good number of observations and the best values of gap and *rms*. This criterion improves the overall quality of the data set and, at the same time, limits undesired effects of redundancy, which may artificially overrate zone a great number of earthquakes with respect those where the distribution of hypocenters is dispersed over wider area.

We obtained, for the successive 1-D inversion, a data-set of 155 well located events with a total of 4,054 P- observations and 2,617 S- observations.

Now we show some the statistics referring to the selected-events quality:

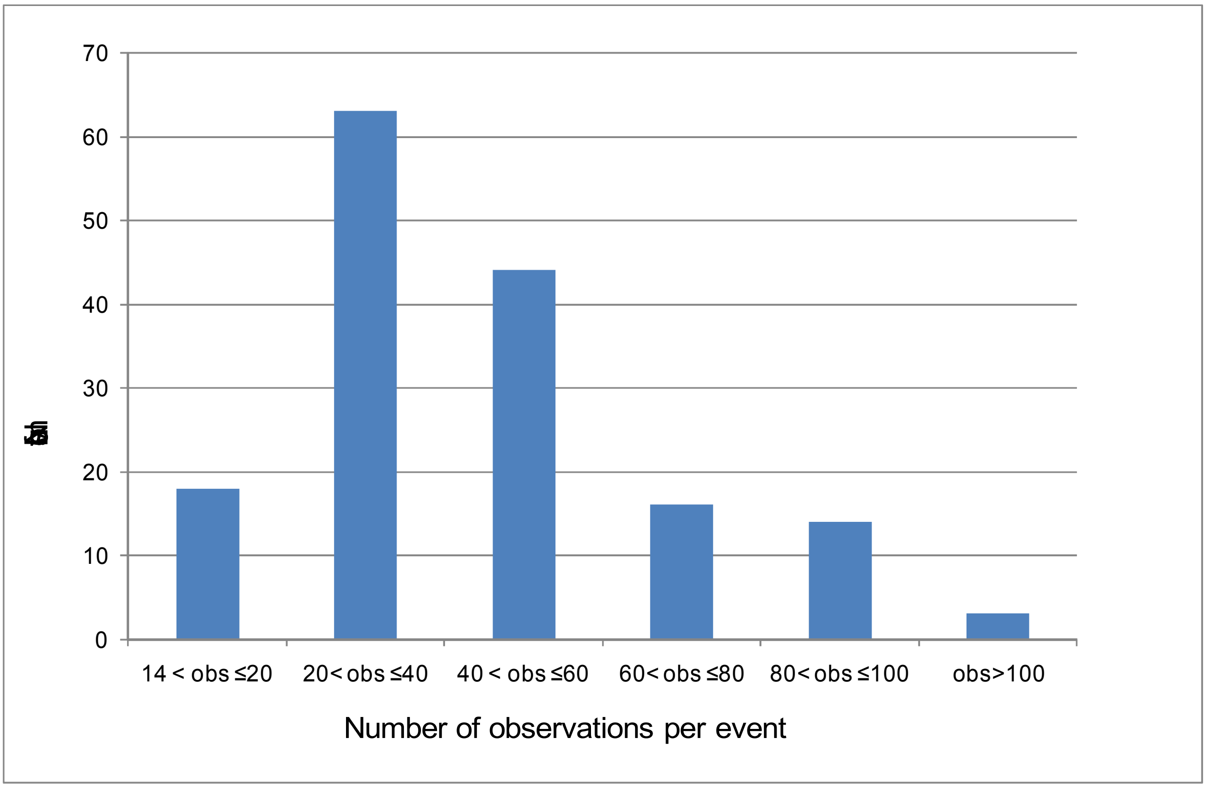

Figure 2.10: Number of observations per event with regards the 155 well located earthquakes. Note that about 50% of the seismic events have more than 40 observations.

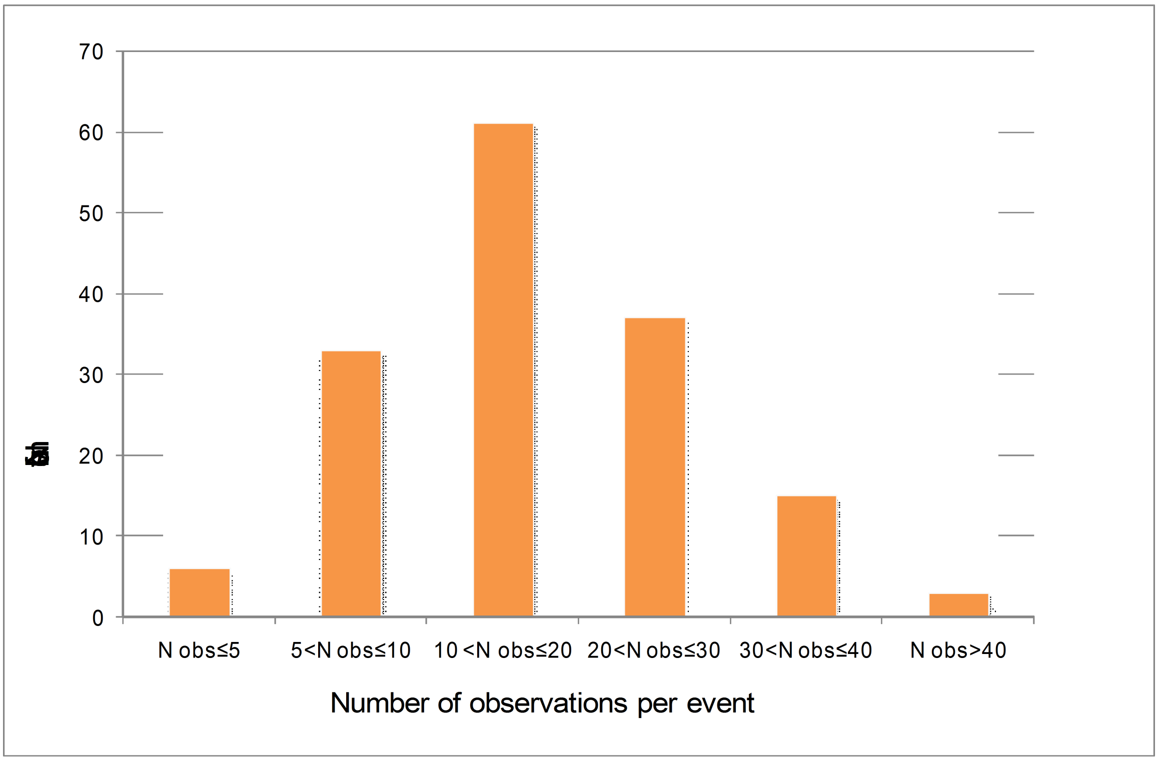

Figure 2.11: Number of S-wave observations per event.

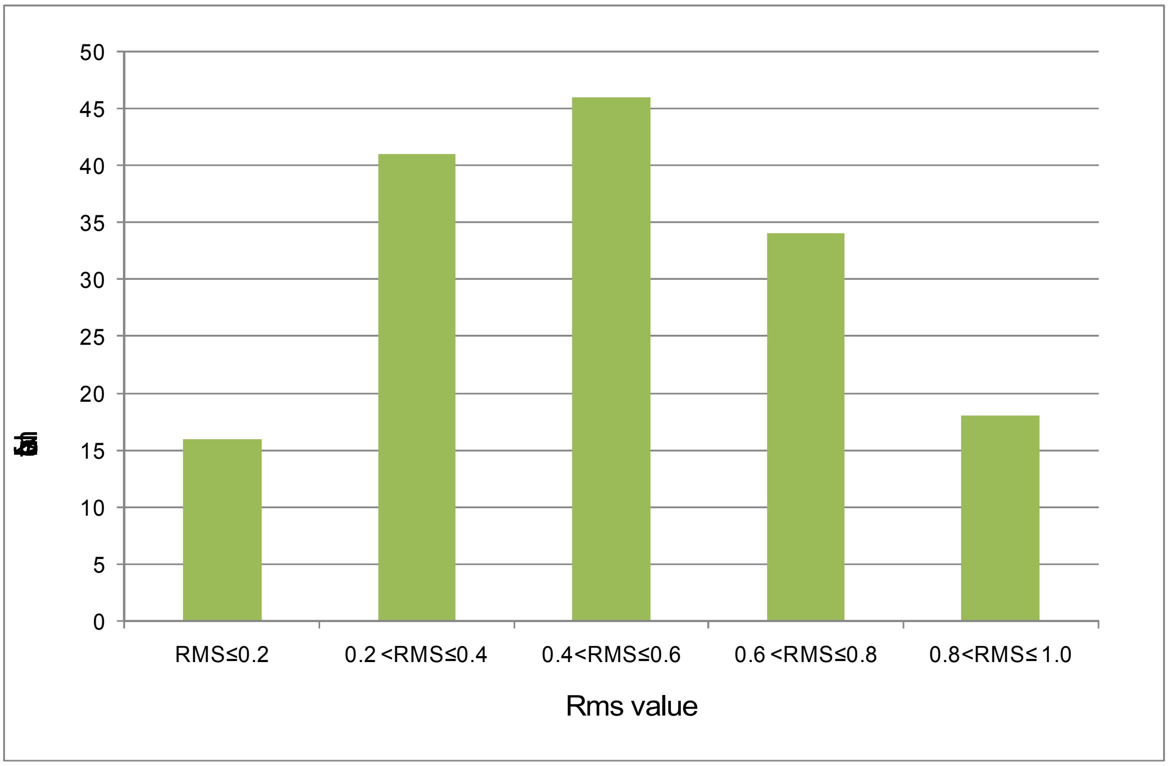

Figure 2.12: Rms distribution. This previous distribution should be improved soon after the 1-D minimum model is constrained, because this one explains part of P- and S- wave residuals.

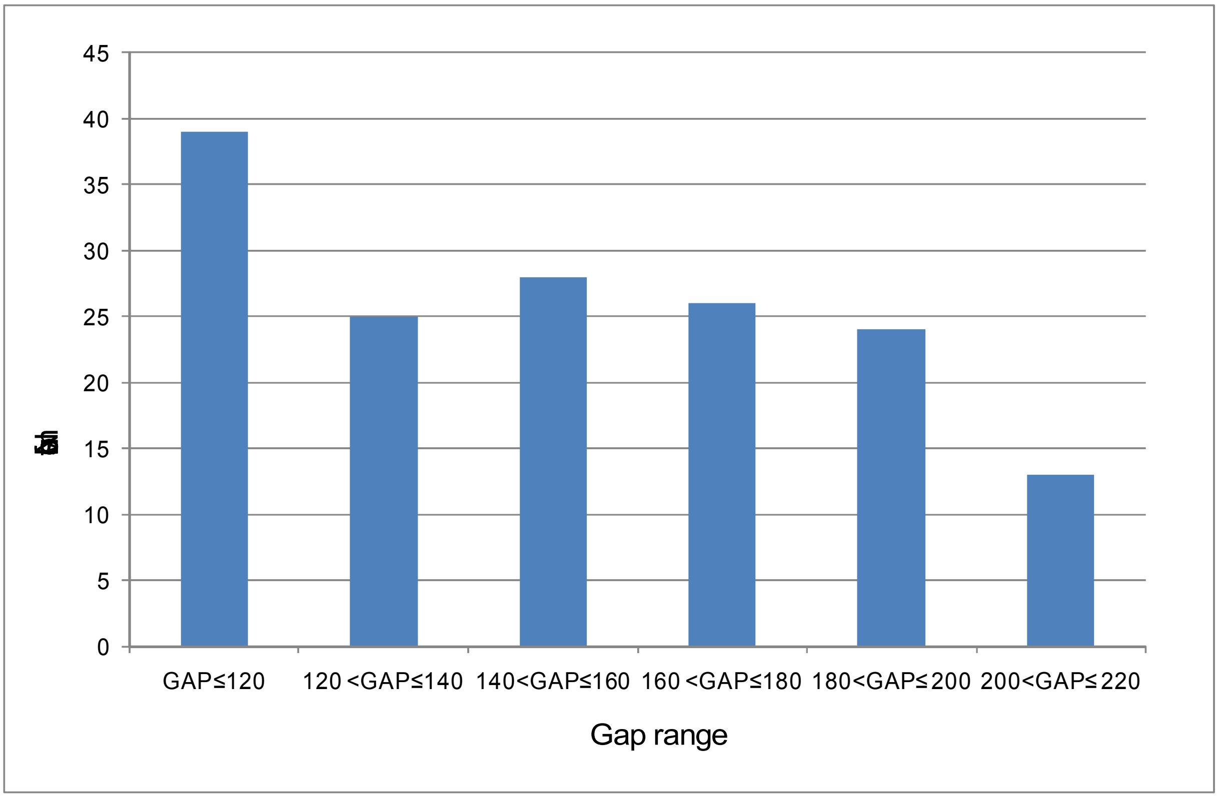

Figure 2.13: Distribution of gap. Note that only 37 seismic events have a gap larger than 180°.

2.6 Magnitudes of the selected events

There are different scales to assess the magnitude of an earthquake. For Charles Richter, which developed the first magnitude scale in 1935, earthquake magnitude (M_L) is the logarithm to the base 10 of the maximum seismic-wave amplitude, in thousandths of a millimeter, recorded on a special type of seismograph (Wood-anderson seismograph) at a distance of 100 km from the earthquake epicenter. The extension of Richter's formula on observations of distant earthquakes led to the definition of new magnitude scales. One such scale, the surface-wave magnitude or M_s scale, is obtained by measuring the largest amplitude in a surface-wave-wave train with a period close to 20 seconds:

$$M_s = \log_{10}(A/T) + 1.66 * \log_{10}(D) + 3.3$$

where A is the amplitude displacement in microns, T the period in seconds and Q an attenuation factor linked to the distance in degrees (D) of the earthquake. Another is the body-wave magnitude or m_b, which is based on the maximum amplitude of teleseismic P waves with a period of about 1 second:

$$m_b = \log_{10}(A/T) + Q\,(D,h)$$

where Q is an attenuation factor linked to the distance in degrees (D) and to the depth in kms (h) of the earthquake.

In our work, magnitude values are obtained from OSVG data-base and derived from Lee's formula by using the programme HYPO71 (Lee et Lahr, 1975):

$$M_d = -0.87 + \log_{10}(D) + 0.0035\delta$$

where D is the seismic signal duration in seconds and δ is the epicentral distance in kms. The M_d value is based on the determination of the signal duration and is generally estimated on several stations of reference (Clément, 2001). The correlation with m_b is given by the following formula:

$$M_d = 0.8 + 0.74\, m_b$$

Figure 2.14 displays the magnitude distribution for 155 events processed in this work. Magnitudes range from 0.5 to 4.4 with an average of 2.3.

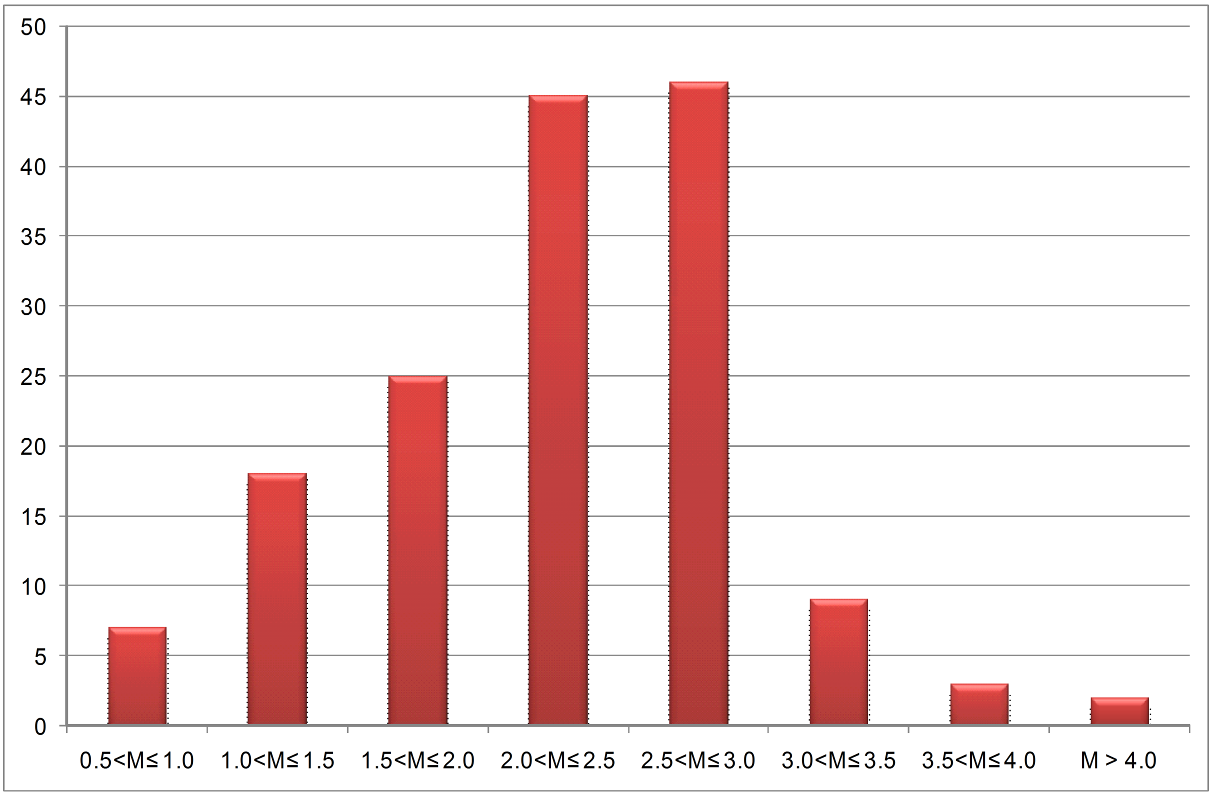

Figure 2.14: Magnitude of the 155 events processed in this work as determined by the OVSG network.

2.7 Hypocentral locations from SISMANTILLES I data

Figures 2.15, 2.16, 2.17 and 2.18 show the earthquake locations of the 155 selected events by using respectively the model 1 and model 2. This earthquake distribution outlines the subduction of the Atlantic seafloor beneath the Caribbean plate and allows us to try to draw the boundary of the plates and the shape of the slab. In particular we present vertical cross-sections (100 km wide) for three profiles perpendicular to the arc. They reveal that the seismicity associated with the subduction slab is clearly observed from 20 to 180 km of depth. We observe, from these profiles, a relatively well-defined Benioff zone that gives an angle of about 45° for the plunge of the slab. We note also that slab position at a depth of 40 km is far more than 70 km from the nearest land station. Indeed, referring to Tohoku subduction zone land stations lie directly above the slab of 40 km depth (Uchida et al., 2010).

On the contrary according to Bengoubou-Valerius et al. (2008), there is no clear dip variation from north to south as a 50° dipping line globally fits the seismic clusters. At a more detailed scale, we clearly see the high seismicity of Marie-Galante graben, which is a major active tectonic structure southeast of Guadeloupe island (Feuillet et al., 2004). Another dense cluster is visible between Antigua and Guadeloupe islands (see also figures 2.8 and 2.9). Should also be remark that the choice of velocity model is important to constrain hypocentral parameters and especially focal depth. Indeed we note that earthquake locations obtained by using the model 2, faster than model 1, are shallower of a few kilometers. All these results of SISMANTILLES I experiment remain preliminary, because they should be improved by 1-D and 3-D inversions.

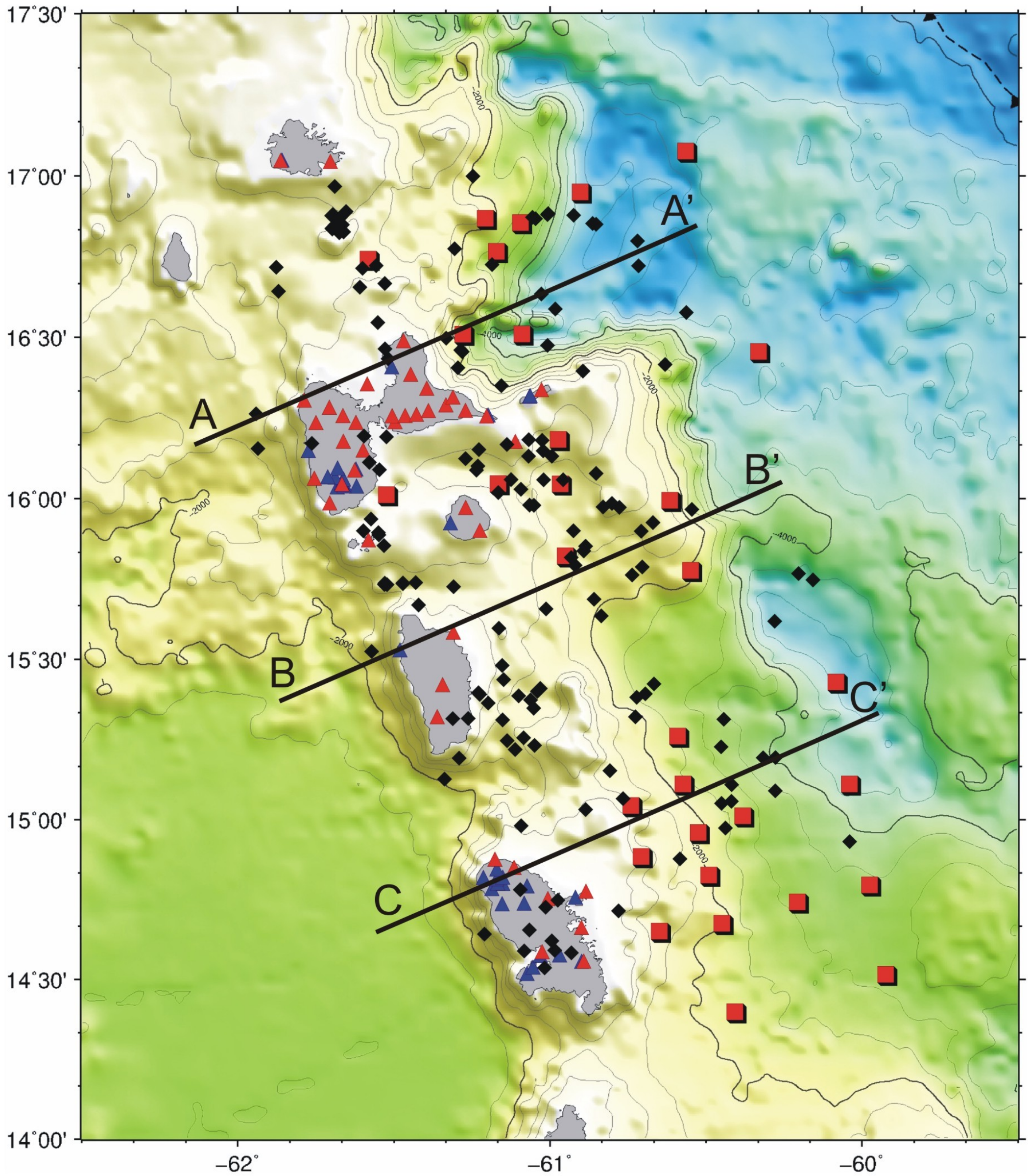

Figure 2.15: Epicentral map of the 155 selected events located with the model 1 (black diamonds). Blue triangles: seismic stations of OVSG; red triangles: temporary seismic stations; red squares: off-shore network. Three seismicity cross sections are taken and presented in figure 2.16. The oceanic trench is represented by dashed line with triangles.

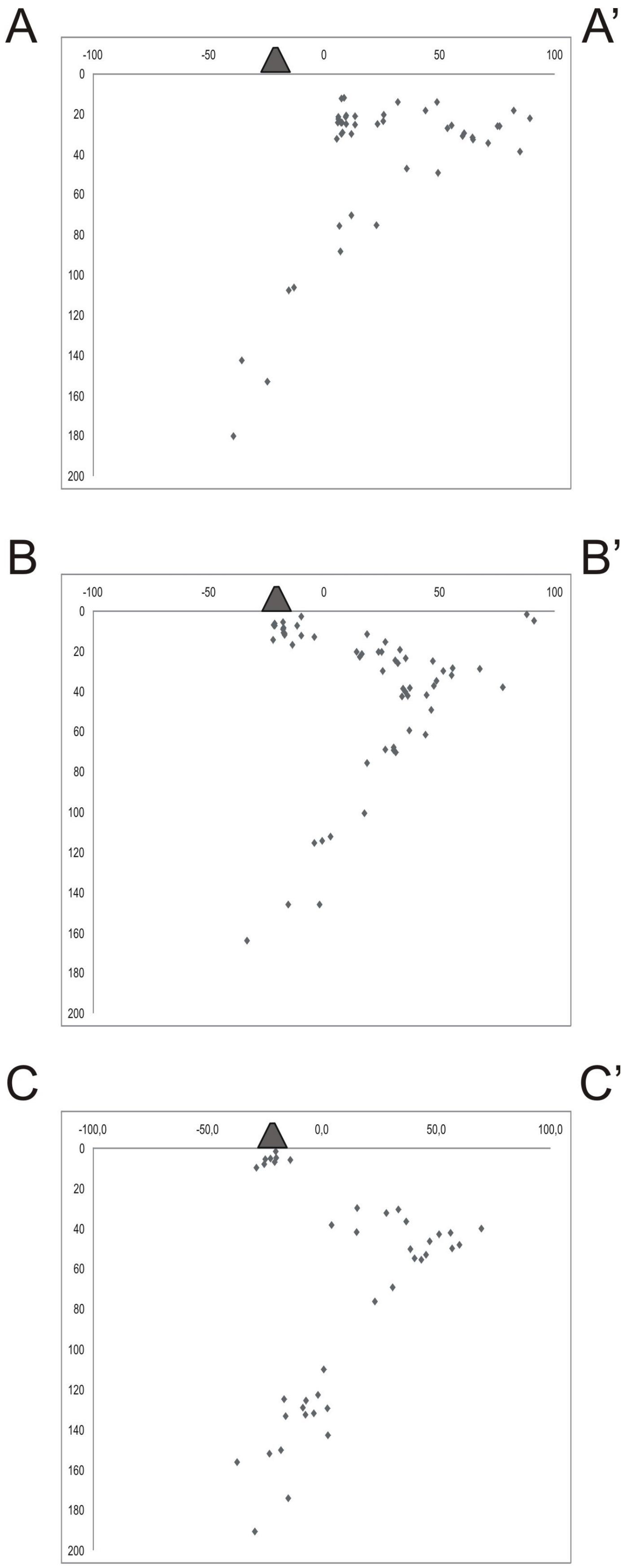

Figure 2.16: Distribution of foci along profiles of figure 2.15.

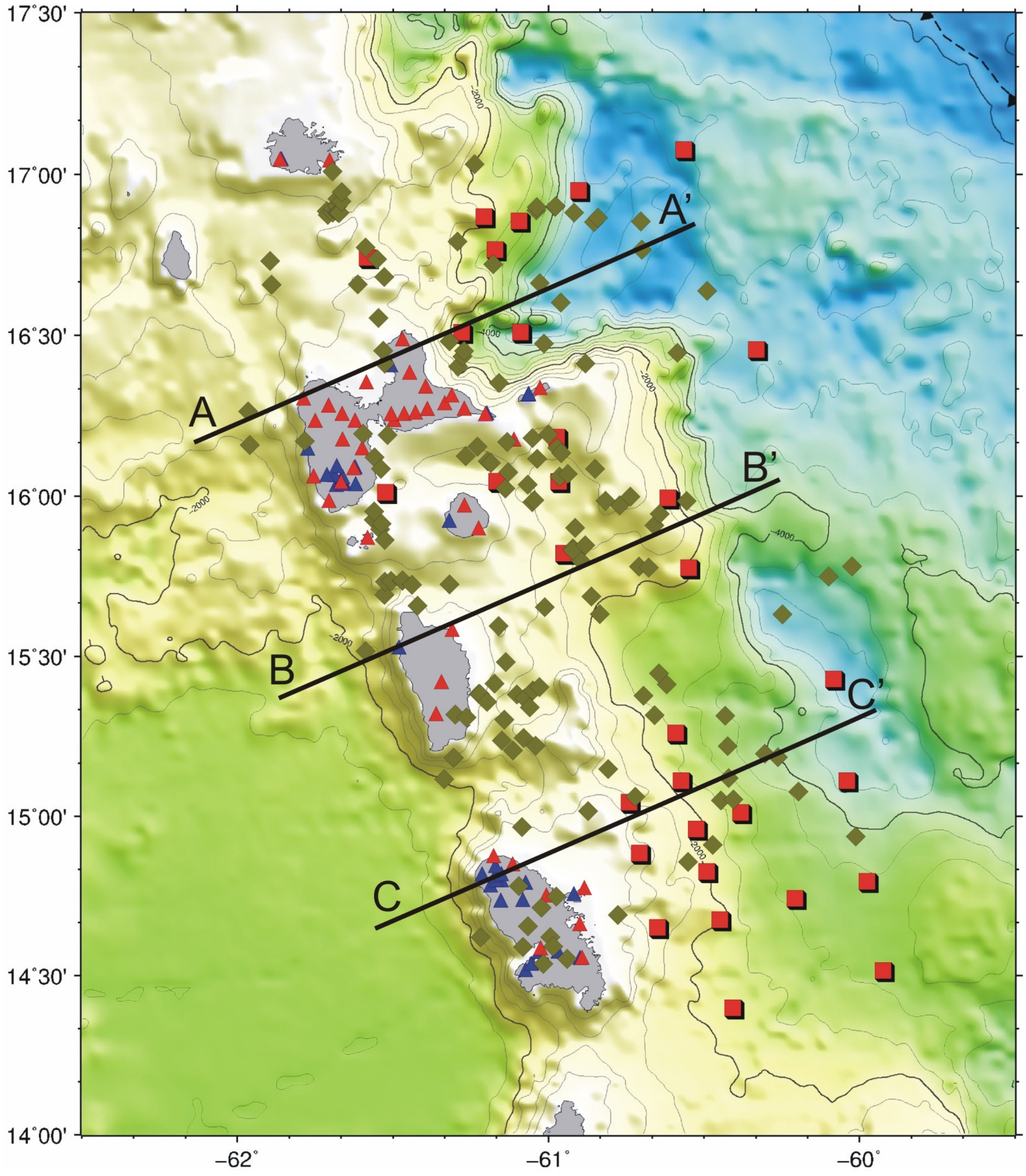

Figure 2.17: Epicentral map of the 155 selected events located with the model 2 (green diamonds). Blue triangles: seismic stations of OVSG; red triangles: temporary seismic stations; red squares off-shore network. Three seismicity cross sections are taken and presented in figure 2.18. The oceanic trench is represented by dashed line with triangles.

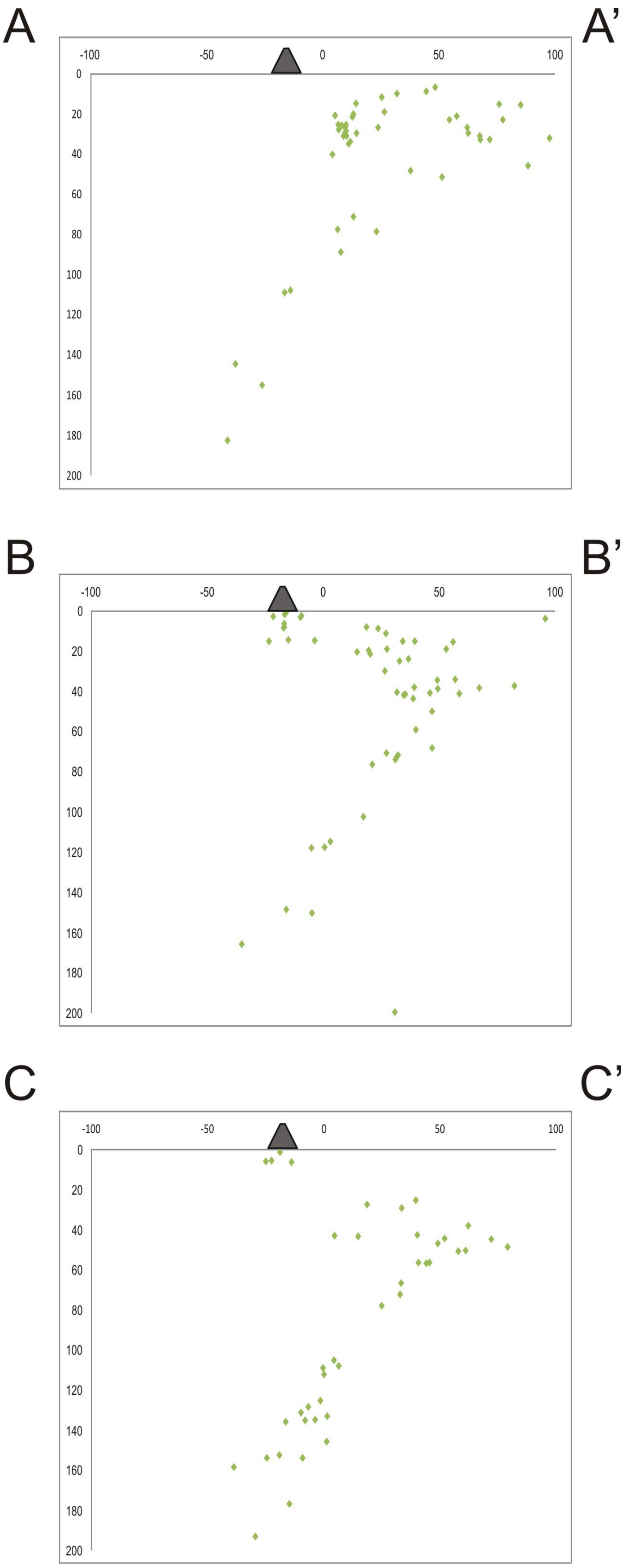

Figure 2.18: Distribution of foci along profiles of figure 2.17.